Supplement of Atmos. Chem. Phys., 25, 13199–13219, 2025
https://doi.org/10.5194/acp-25-13199-2025-supplement

Atmospheric Chemistry and Physics
Open Access

Supplement of

Dust radiative forcing in CMIP6 Earth System models: insights from the AerChemMIP piClim-2xdust experiment

Ove W. Haugvaldstad et al.

Correspondence to: Ove W. Haugvaldstad (oveh@met.no)

S1 Supplementary Text

S1.1 Conversion to equivalent precipitation units

In Figure 4, we display the atmospheric radiative cooling (ARC) in terms of equivalent precipitation units of mm year^{-1}. To convert ARC from units of Wm^{-2} to equivalent precipitation units in mm year^{-1}, we calculate the total energy absorbed by the atmosphere over one year:

$$\text{Total Energy over a year} = \text{ARC}[W\,\text{m}^{-2}] \times 31,536,000$$

Then we calculate the theoretical maximum of water that can be evaporated:

$$\text{mass} = \frac{\text{ARC}[W\,\text{m}^{-2}] \times 31,536,000}{L}$$

Where L is the latent heat of vaporisation that is approximately equal to 2260×10^3 Jkg^{-1}. Next, we convert the mass of evaporated water into volume:

$$\text{Volume} = \frac{\text{mass}}{\rho}$$

With the mass of water $\rho = 1000, \text{kg/m}^3$. Lastly, we convert the volume into precipitation equivalent in mm:

$$h\,[\text{mm}] = \left(\frac{\text{ARC}[W\,\text{m}^{-2}] \times 31,536,000}{2260000}\right) \times 1000$$

$$\text{Precipitation Equivalent ARC (mm/year)} = \frac{\text{ARC}[W\,\text{m}^{-2}] \times 31,536,000}{2260000}$$

S2 Supplementary Figures

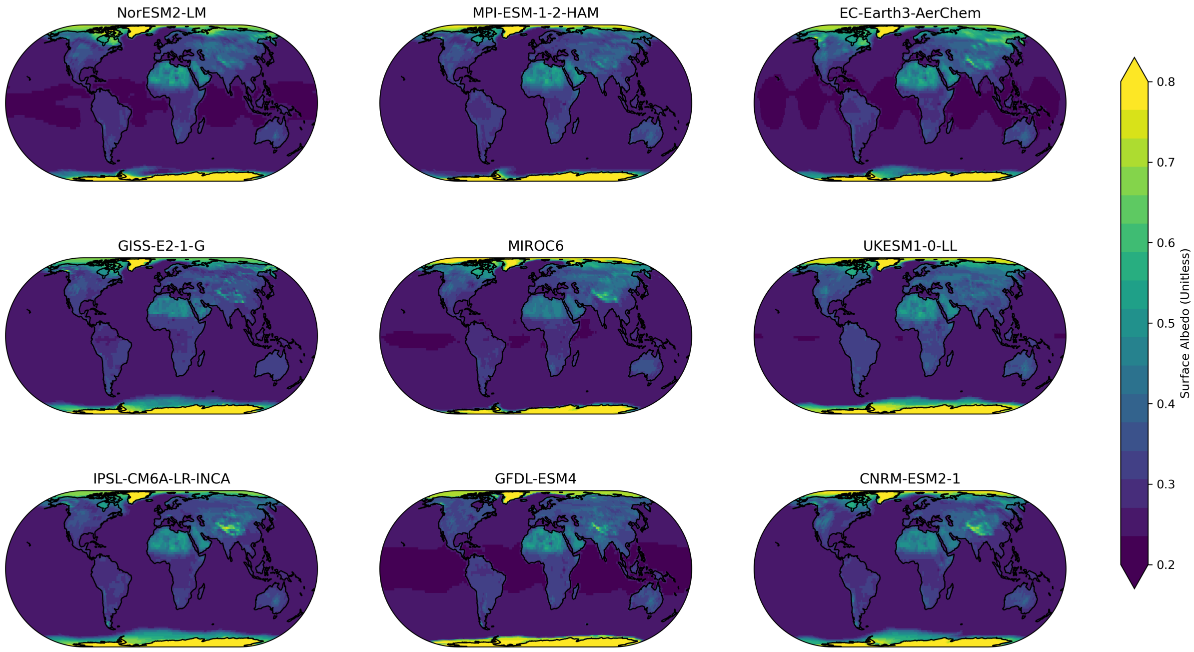

Figure S1: Map of Surface albedo (unitless) for each of the nine AerChemMIP models used.

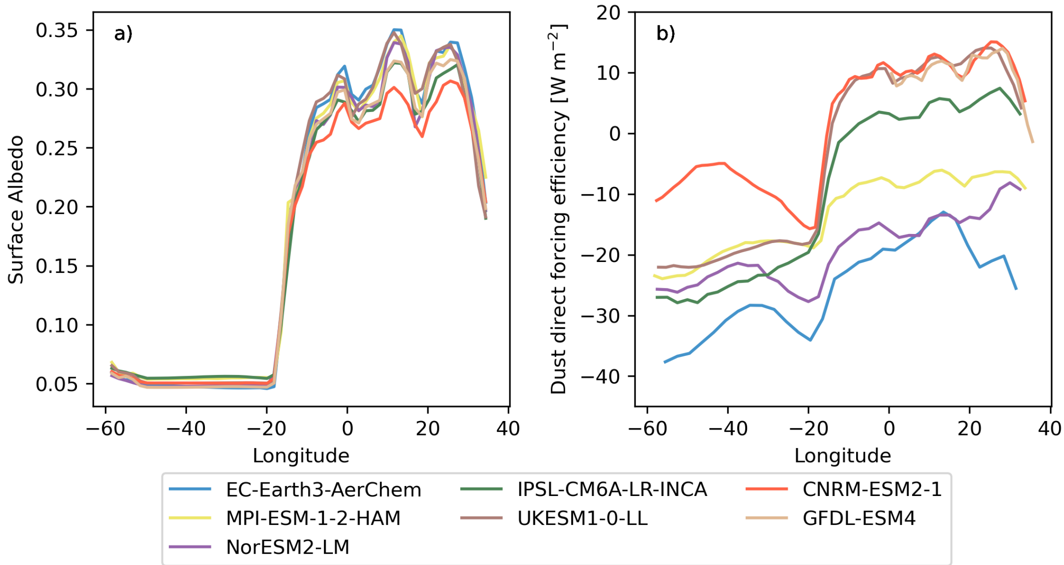

Figure S2: **(a)** Surface albedo and **(b)** dust direct forcing efficiency per unit of AOD averaged between 5°– 31°N. The zonal extent of the area includes the Sahara (high albedo over desert) and North Atlantic (low albedo over ocean).

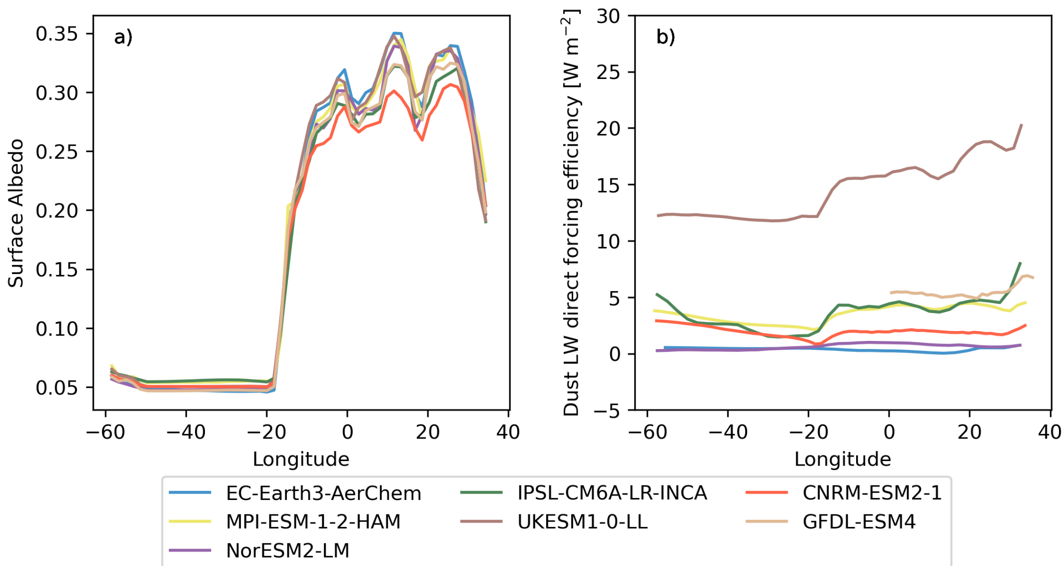

Figure S3: As Figure S1, except showing the longwave direct forcing efficiency only.

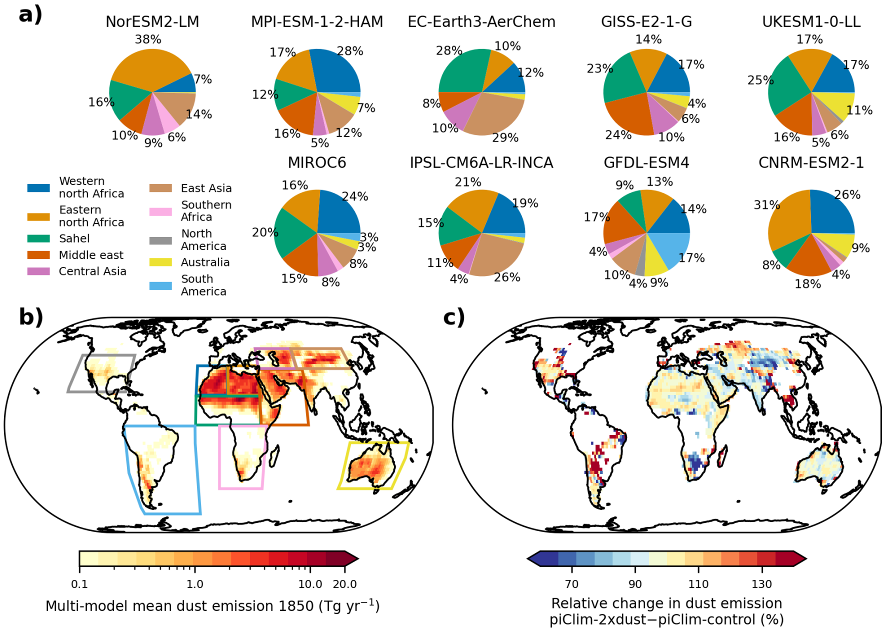

Figure S4: **(a)** The relative change in *piClim-2xdust* from *piClim-control* in dust emission from different dust emitting regions the regional extent of each region is indicated in panel b. **(b)** *piClim-control* multi-model mean dust emission flux (Tg year^{-1}), the rectangle show key dust emission regions according to Kok et al. (2021). **(c)** The multi-model mean change in dust emissions of *piClim-2xdust* relative to the *piClim-control*.

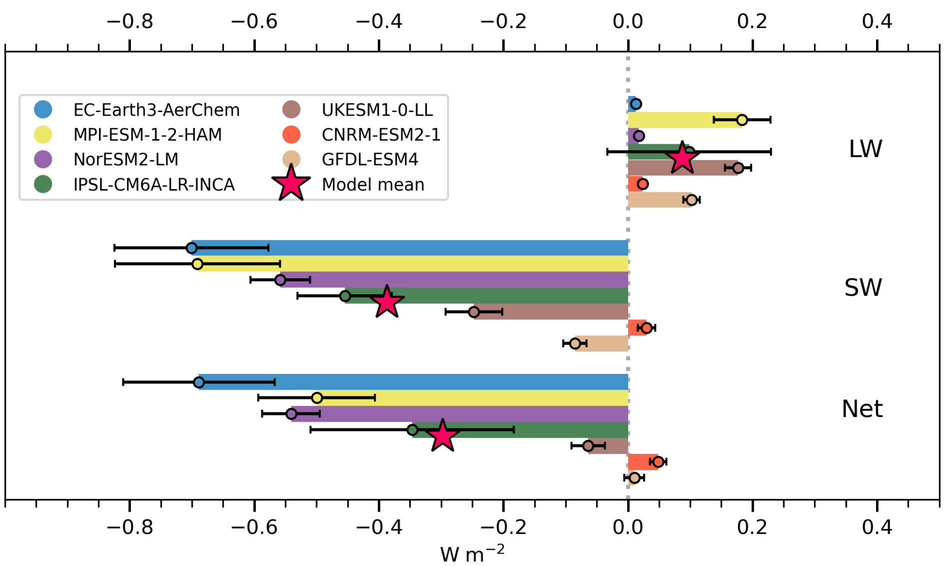

Figure S5: Dust direct effective radiative effect (W m^{-2}). The direct effective radiative effect is the DuERF from *piClim-2xdust* minus *piClim-control*, scaled up or down to match a 100% increase in dust burden.

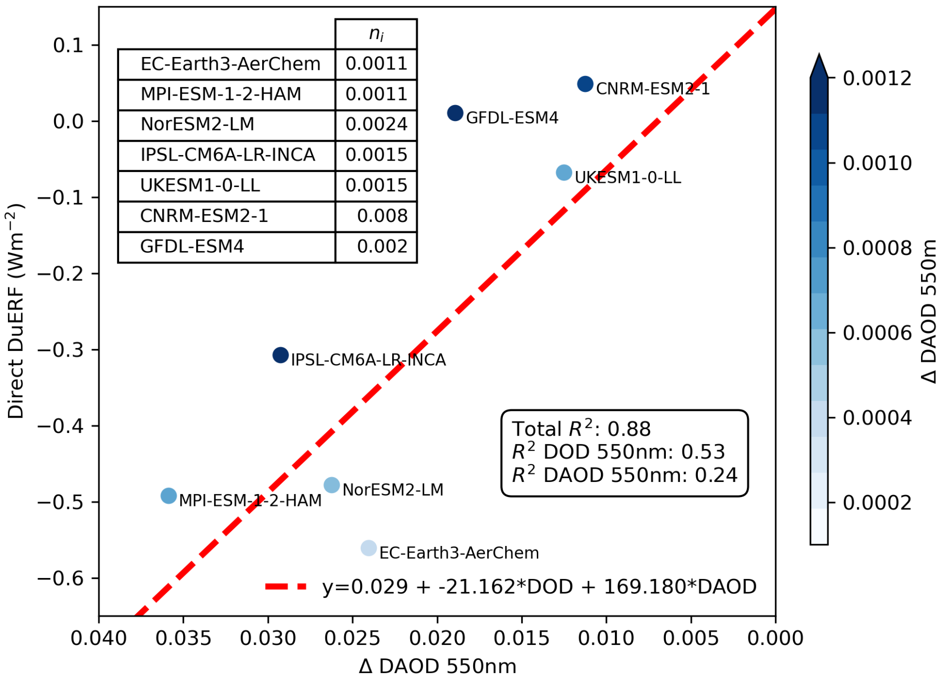

Figure S6: Change in DOD *piClim-2xdust* vs *piClim-control* (x-axis) and direct dust effective radiative forcing (y-axis). The colouring shows the change in DAOD. The table show the complex index of refraction at 550nm for the models. The red stippled line shows the multiple linear regression line. The r-squared values for the linear fit using DOD 550nm, DAOD 550nm and both are written out in the round text box.

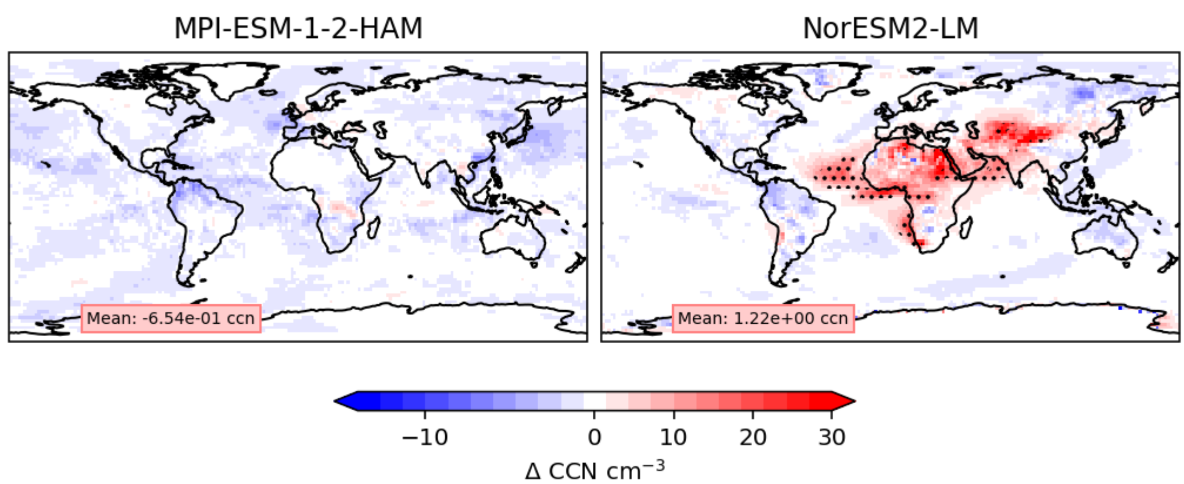

Figure S7: Absolute change in CCN concentration between *piClim-2xdust* and *piClim-control*, for MPI-ESM-1-2-HAM and NorESM2-LM.

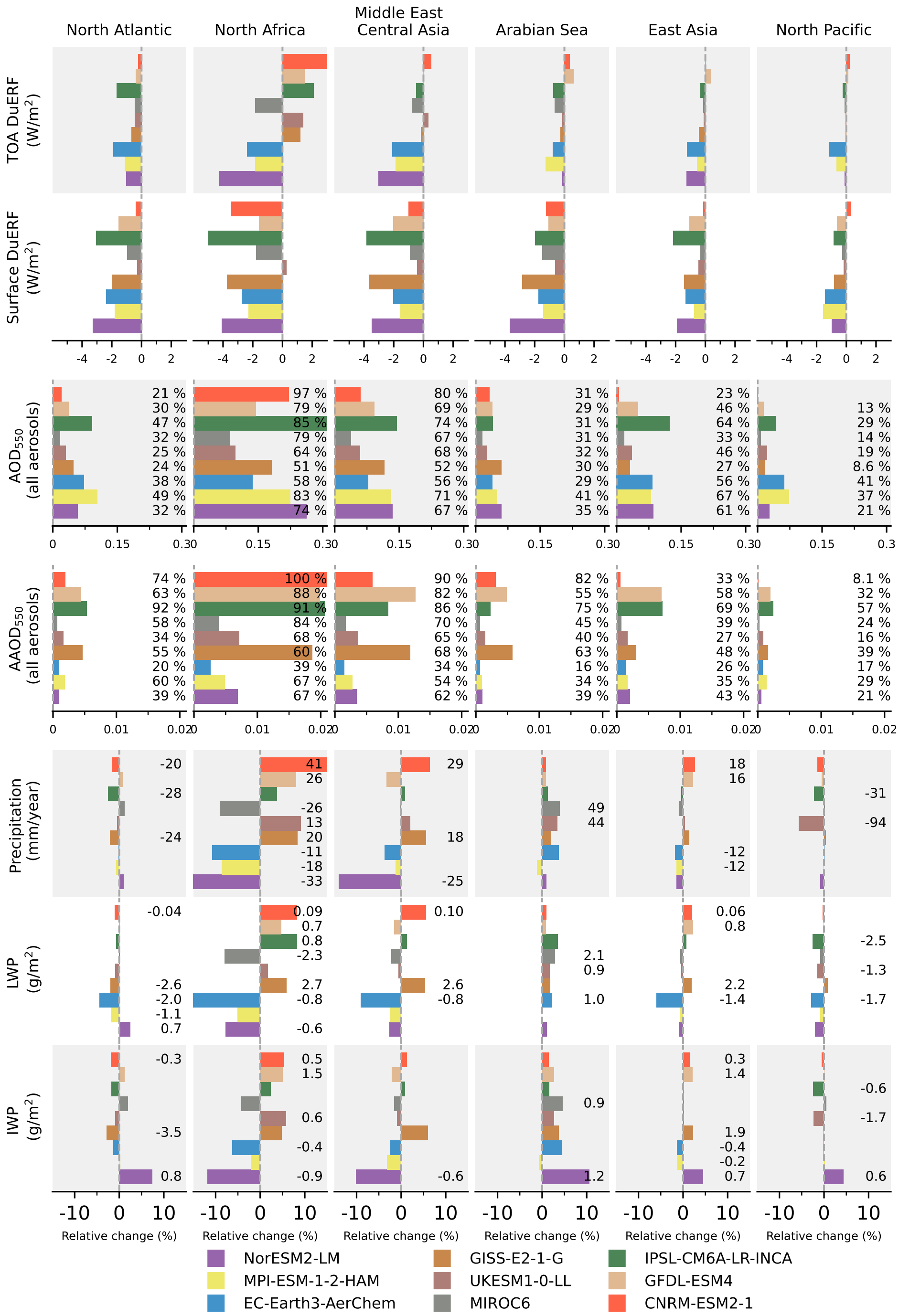

Figure S8: The difference between *piClim-control* and *piClim-2xdust* for key dust outflow regions; North Atlantic (6°S - 34°N, 66°W - 16°W), Arabian Sea (6°S - 19°N, 19°E - 82°E) and North Pacific (15°N - 48 °N, 117°E - 147°E) and dust sources: North Africa (10°N - 31°N, 14 °W - 37 °E), Middle East and Central Asia (19°N - 44 °N, 37°E - 79°E) and East Asia (23°N - 61°N, 117°E - 147°E). From top to bottom; Dust Effective radiative forcing at TOA and surface, AOD and AAOD at 550nm, Precipitation, Liquid water path (LWP) and Ice water path (IWP). The bars in the top four panels show absolute changes, while in the bottom 3 panels the bars indicate the relative change. The value of the changes that are significant in panels 2-5 are displayed.

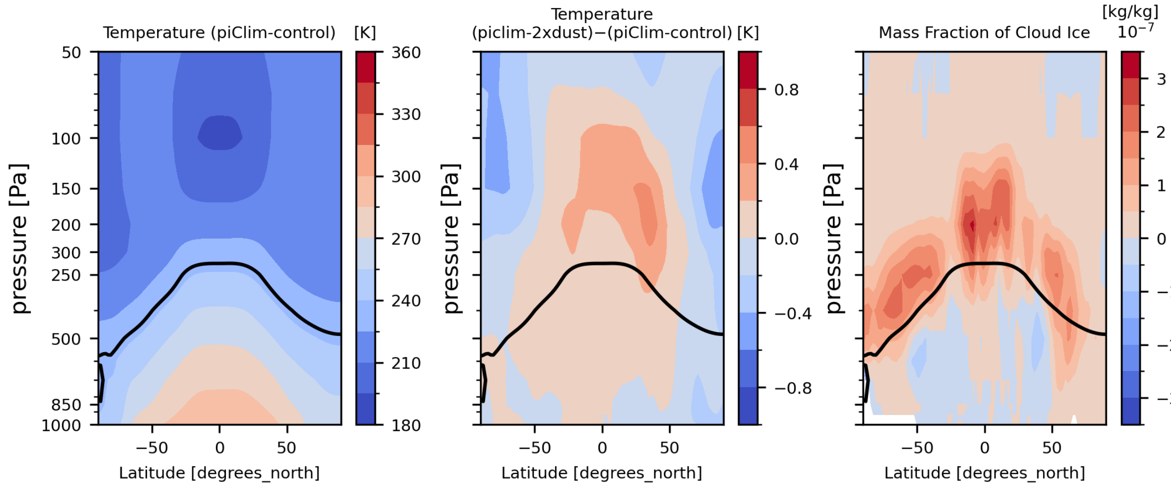

Figure S9: Zonal plot of NorESM2-LM *piClim-control* temperature, change in temperature between *piClim-control* and *piClim-2xdust* and change in ice mass fraction (kg/kg). The black solid line highlights the −37°C isotherm, which indicates the transition between the mixed-phase and cirrus cloud regimes.

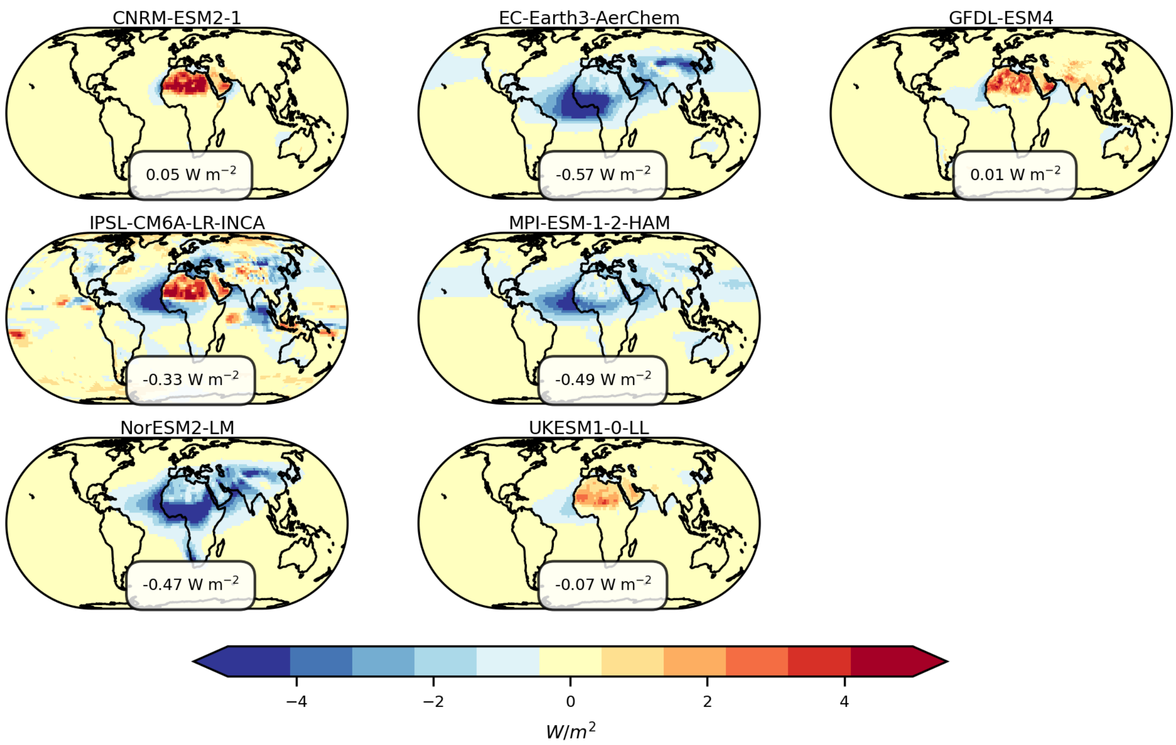

Figure S10: The direct term of dust effective radiative forcing according to the Ghan (2013) decomposition; the global mean value is written in text box.

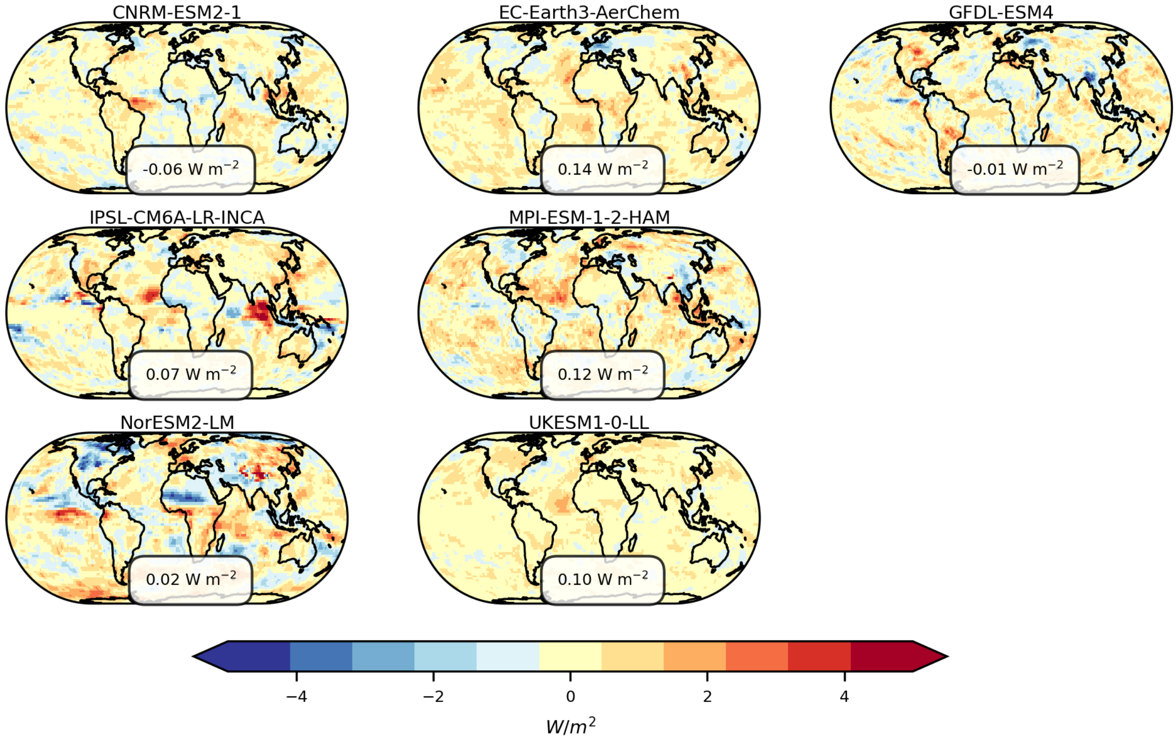

Figure S11: The cloud term of dust effective radiative forcing according to the Ghan (2013) decomposition; the global mean value is written in text box.

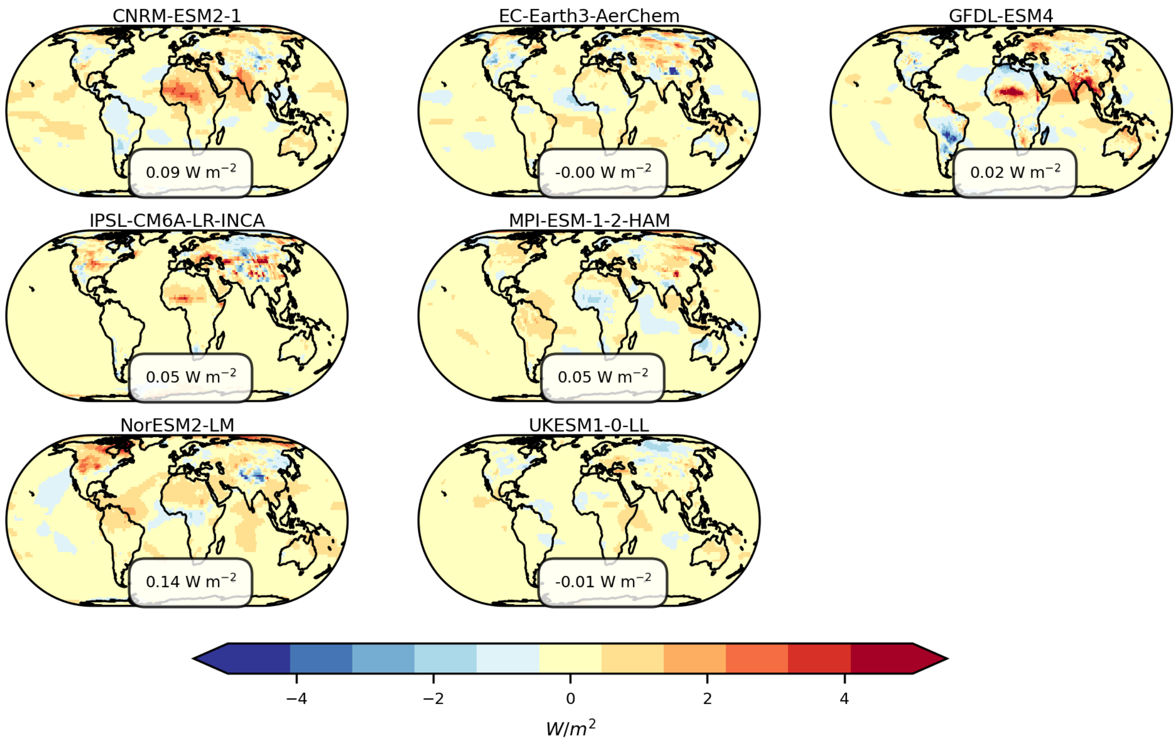

Figure S12: The albedo term of dust effective radiative forcing according to the Ghan (2013) decomposition; the global mean value is written in text box.

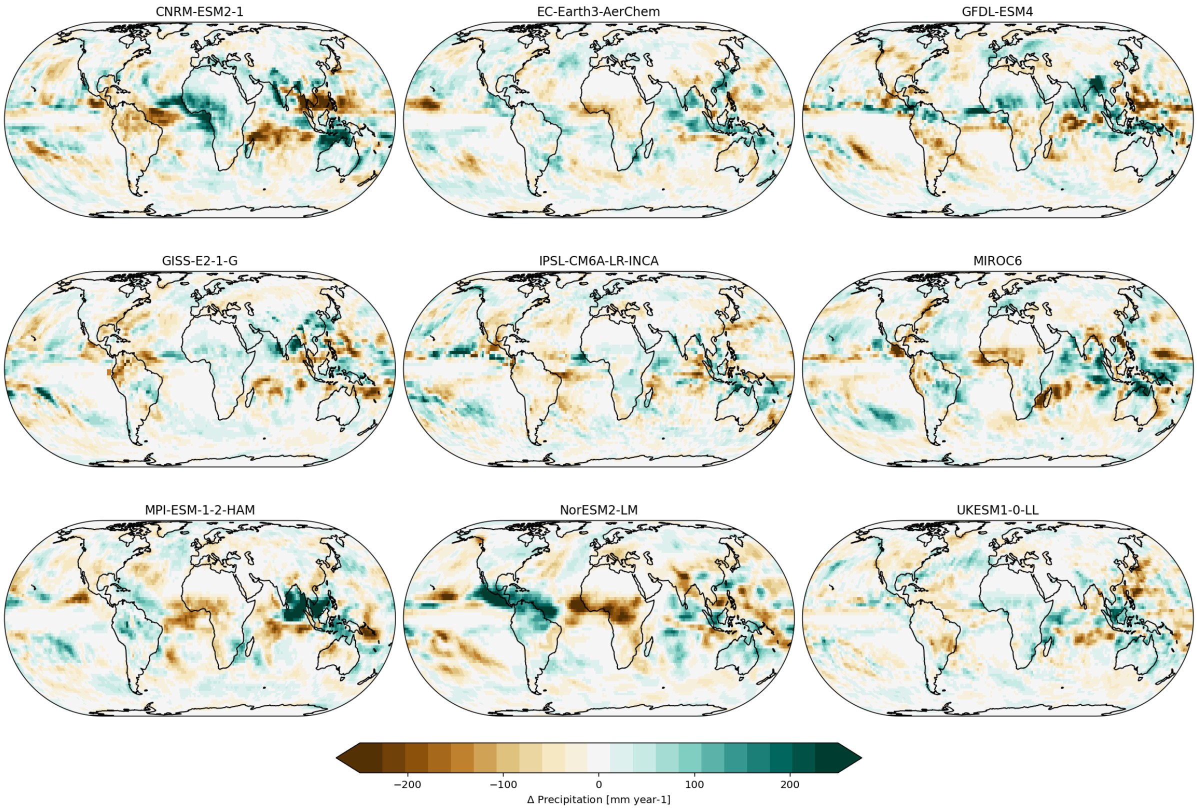

Figure S13: Change in precipitation between *piClim-2xdust* and *piClim-control*

References

Ghan, S. J.: Technical Note: Estimating aerosol effects on cloud radiative forcing, Atmospheric Chemistry and Physics, 13, 9971–9974, https://doi.org/10.5194/acp-13-9971-2013, 2013.

Kok, J. F., Adebiyi, A. A., Albani, S., Balkanski, Y., Checa-Garcia, R., Chin, M., Colarco, P. R., Hamilton, D. S., Huang, Y., Ito, A., Klose, M., Li, L., Mahowald, N. M., Miller, R. L., Obiso, V., Pérez García-Pando, C., Rocha-Lima, A., and Wan, J. S.: Contribution of the world's main dust source regions to the global cycle of desert dust, Atmospheric Chemistry and Physics, 21, 8169–8193, https://doi.org/10.5194/acp-21-8169-2021, publisher: Copernicus GmbH, 2021.